Derisking Development by a Cocrystallization Screen of a Novel Selective Inhaled JAK-STAT inhibitor

Antonio Llinas,[§] Rafael Barbas,[†] Mercè Font-Bardia,[‡] Amir Smailagic,[§] and Rafel Prohens[†,‖]

§ Respiratory Inflammation and Autoimmunity IMED Biotech Unit, AstraZeneca, Gothenburg, Sweden

†Unitat de Polimorfisme i Calorimetria, Centres Científics i Tecnològics, Universitat de Barcelona, Baldiri Reixac 10, 08028 Barcelona, Spain

‖Center for Intelligent Research in Crystal Engineering S.L, Palma, Spain

‡Unitat de Difracció de Raigs X, Centres Científics i Tecnològics, Universitat de Barcelona, Barcelona, Spain

Antonio Llinas Antonio.Llinas@astrazeneca.com

Rafel Prohens rafel@ccit.ub.edu

ABSTRACT:

The discovery and detailed characterization of several new solid forms of a novel selective inhaled JAK-STAT inhibitor are described. Using a holistic cocrystallization screen approach to explore its formulation landscape, we decrease the risk of future potential development failures due to a nonoptimal pharmacokinetic lung profile or undesired lung effects in humans.

..

1. INTRODUCTION

Compound 1 is a novel and selective Janus kinase-signal transducers and activation of transcription (JAK-STAT) inhibitor. JAKs belong to one intracellular subgroup of the nonreceptor protein tyrosine kinases involved in cell growth, survival, development, and differentiation of a variety of cells, critically important for immune and hematopoietic cells. Type I and II cytokine receptors are constitutively associated with JAKs, and the binding of ligand (cytokine) initiates a transphosphorylation cascade: receptor-JAK-STAT. Phosphorylated STATs dissociate from the receptor, dimerize, translocate to the nucleus, and bind to specific sequences to regulate the expression of target genes.1,2
Given the importance of JAKs inhibitors ("jakinibs") to modulate cytokine signaling, they may be useful for the treatment of various diseases or conditions in which the functions of the innate and/or adaptive immune system are involved.3−5 JAK inhibitors are currently being evaluated in a diverse range of disorders (rheumatoid arthritis, psoriasis, inflammatory bowel disease, and myeloproliferative disorders), and many more trials are underway in other autoimmune disorders (juvenile idiopathic arthritis, ankylosing spondylitis, systemic lupus erythematosus, Sjögren's syndrome), chronic kidney disease and diabetic nephropathy, breast cancer, lymphoma, and the prevention of graft rejection. For a review of the pharmaceutical intervention of the JAK/STAT pathway, see references 6−9.

In view of the numerous conditions and disorders susceptible to "jakinibs" treatment, it is expected that the new compounds, new forms of an existing compound, and new routes of administration for these compounds provide significant therapeutic benefits to a variety of patients.

When developing poorly soluble drugs for oral inhaled delivery, special caution needs to be paid to the design of the inhalation product. For inhaled compounds, the mean absorption time from the lung is not usually correlated to a single physicochemical property,10 but there is some evidence that the absorption from the lung of a poorly soluble neutral inhaled compound into the central circulation may be correlated to dissolution.11 Controlling the dissolution rate is therefore of utmost importance to achieve an optimal lung pharmacokinetic profile. When a poorly soluble inhaled compound dissolves too fast, the desired effect can be too short, assuming neither permeability nor transporter cell uptake is limiting the absorption. On the other hand, if it dissolves too slowly, the compound might accumulate in the lung and be a reason for unexpected adverse effects. The rate and extent of the absorption from the lung (and the safety profile) of a poorly soluble inhaled compound will depend (excluding physiological differences or disease-related changes) on many factors, mainly the physicochemical properties of the delivered drug and its material properties (solubility, dissolution rate, size, shape, charge, crystallinity, and chemical composition). It is generally accepted that any undissolved particulate material in the lungs can result in adaptive adverse/ tox effects.12 It is therefore advisable to explore the formulation landscape as early as possible in the discovery phase so several forms (salts, cocrystals, solvates,

polymorphs···), with different physicochemical properties, are available to the team for in vivo assessment and in this way decrease the risk of costly surprises during the following development phase.

In this paper, we describe the discovery and detailed characterization of several new forms of 1 using a holistic approach to explore the formulation landscape of 1 to decrease the risk of potential development failures due to a nonoptimal pharmacokinetic lung profile or undesired lung effects in humans. To do so, we selected a list of 20 coformers from a database containing more than 2300 compounds, including 860 products regarded as "safe" by the FDA (GRAS list). The selection was performed according to the virtual prediction results in combination with a factor obtained from a multiparameter assessment, which included melting point of the coformers, safety and tox profile of the coformers, and solubility in water stipulation. We gave an important relative weight to the safety/tox profile for each coformer, since the new forms discovered were intended for human use. The safety/tox profile was performed as a combination of an in house AZ in silico assessment, experimental safety end points from multiple databases, and different structural alerts. The resulting safety/tox profile contained information about hERG activity, phospholipidosis, AhR, Nav1.5, CaV1.2, potential to form reactive metabolites, genotox, AMES, carcinogenicity, mouse lymphoma, chromosomal aberration and micro nucleus, among others. The solubility stipulation was assigned a high contribution factor to the multiparameter assessment since it had been shown previously that the solubilities of compounds formulated as cocrystals increase in proportion to the solubility of the coformer.13,14 The experimental cocrystal screen was then performed on 20 coformers with a good chance of forming a cocrystal with different, and hopefully better, dissolution rate profiles (compared to the free base 1), which are stable and safe for human oral inhaled dosing.

2. MATERIALS AND METHODS

2.1. Experimental Screen. A comprehensive cocrystal screening has been conducted by using different combinations of solvents at several concentrations and temperatures, with variable cooling rates, in both thermodynamic and kinetic conditions. Solubility of 1 was initially determined in 36 solvents, and accordingly drop grinding, reaction crystallization, and solved mediated transformation techniques were applied to each 1/coformer combination. All solids were analyzed by powder X-ray diffraction (PXRD) to assess the formation of a new solid form.

2.2. Virtual Cocrystal Screening. For each compound, the molecule was drawn in an extended conformation and energy minimized using the molecular mechanics methods implemented in TorchLite.15 Gaussian 09 was used to optimize the geometry and calculate the MEPS on the 0.002 Bohr Å−3 electron density isosurface using density functional theory (DFT) and a B3LYP/6-31G* basis set.16 The MEPS was converted into SSIPs using in-house software.17

2.3. Powder X-ray Diffraction (PXRD). Powder X-ray diffraction patterns were obtained on a PANalytical X'Pert PRO MPD diffractometer in transmission configuration using Cu Kα1+2 radiation (λ = 1.5418 Å) with a focalizing elliptic mirror, a PIXcel detector working at a maximum detector's active length of 3.347°. Flat geometry has been used for routine samples sandwiched between lowabsorbing films (polyester of 3.6 μm of thickness) measuring 2θ/θ scans from 2 to 40° in 2θ with a step size of 0.026° and a measuring time of 80−300 s per step. The indexation of the PXRD diagrams was carried out by means of Dicvol04.18 The unit cell parameters were refined by Le Bail fit19 using the Fullprof program,20 and the most probable space groups were determined from the systematic absences.

2.4. Differential Scanning Calorimetry (DSC). Differential scanning calorimetry analyses were carried out by means of a Mettler- Toledo DSC-822e calorimeter. Experimental conditions: aluminium crucibles of 40 μL volume, atmosphere of dry nitrogen with 50 mL/min flow rate, heating rate of 10 °C/min. The calorimeter was calibrated with indium of 99.99% purity. (m.p.: 156.8 °C ΔH: 28.68 J/g).

2.5. Thermogravimetric Analysis (TGA). Thermogravimetric analyses were performed on a Mettler-Toledo TGA-851e thermobalance. Experimental conditions: alumina crucibles of 70 μL volume, atmosphere of dry nitrogen with 50 mL/min flow rate, heating rate of 10 °C/min.

2.6. X-ray Crystallographic Analysis. The single crystal structures were collected using a D8 Venture system equipped with a multilayer monochromator and a Mo or Cu microfocus (λ = 0.71073 Å or λ = 1.54178 Å) has been used too. Frames were integrated with the Bruker SAINT software package using a SAINT algorithm. Data were corrected for absorption effects using the multiscan method (SADABS).21 The structures were solved and refined using the Bruker SHELXTL Software Package, a computer program for automatic solution of crystal structure and refined by fullmatrix least-squares method with ShelXle Version 4.8.0, a Qt graphical user interface for the SHELXL computer program.22

3. RESULTS AND DISCUSSION

3.1. Virtual Cocrystal Screen. The selection of the coformers used in the cocrystal screen was based on the computational cocrystal screen method developed by Prof. Hunter, which has been validated using experimental cocrystal data extracted from the literature.23,24 This computational method has been recently applied to several active pharmaceutical ingredients (APIs) with a remarkable success by Hunter's group, including nalidixic acid,25 griseofulvin and spironolactone,26 and some of us have recently used it to guide the discovery of new cocrystals of zafirlukast27,28 and sildenafil.29 The in silico method is based on the calculation of a cocrystal pairing energy between the API and the coformer. This calculation is performed by using the surface site interaction points (SSIPs), which can be extracted from molecular electrostatic potential surfaces computed at the DFT level of computation as described in reference 17 or estimated with a faster method based on the molecular electrostatic potential surfaces (MEPS) calculated from MMFF94 atomic partial charges.30,31 We have followed the methodology at the DFT level of computation with compound 1, and 20 coformers have been chosen among the 100 coformers with the highest probability of cocrystallization from a database containing more than 2400 compounds (including 860 products from the GRAS list) according to the virtual prediction ranking. Table 2 shows the 20 coformers along with their corresponding ΔE values.

The so-called "rule of 3" is frequently used to predict the outcome of a salt or a cocrystal. The rule is based on the calculation of the difference of pKa between the protonated base and the acid. When this value is less than 0, a cocrystal is expected, and when it is greater than 3 a molecular salt is the expected form. However, with intermediate values predictions are less reliable.32,33 Recently, a linear relationship between the ΔpKa value and the probability of salt/cocrystal formation has been derived by Cruz-Cabeza from more than 6000 component systems (eq 1).34 This equation allows a statistical prediction of proton transfer (P, %) around the "salt-cocrystal continuum" region of ΔpKa ≈ 1, which lies in a range of values between −1 and 4. We have applied this simple calculation to the coformers chosen for the screening in order to assess the probability of proton transfer, and values can be found in Table 2.

$$P(\%) = 17\,\Delta pK_a + 28 \text{ for } -1 \leq \Delta pK_a \leq 4 \quad (1)$$

Given that 1 contains a pyrimidine and a benzoxazolinone group (measured pKa values of 5.9 and 8.9 respectively) and most of the coformers are carboxylic acids and strong organic bases, according to the pKa rule, both salts and cocrystals were expected to be obtained, although with a higher probability of salt formation. However, since both types of multicomponent solid forms could improve hysicochemical properties, no coformers were filtered according to proton transfer probability in order to increase diversity of crystal forms.

3.2. Experimental Salt/Cocrystal Screen. A total number of 130 experiments using selected combinations between 36 solvents and 20 coformers have been conducted, distributed mainly in two methodologies (drop grinding and reaction crystallization techniques) to test the formation of cocrystals with compound 1. Our high-throughput methodology consists of the initial and qualitative solubility assessment of compound 1 and each of the 20 coformers in 36 solvents.36 Then, four solvents were selected according to the solubility information, which is a key issue for a rational design of the screening conditions and that allows the optimized exploration of the cocrystallization landscape for each 1/conformer combination with the highest probability of success and the lowest number of experiments. Evidence of cocrystallization is detected by measuring PXRD diffractograms and DSC thermograms for each solid obtained during the screen. When it has not been possible to solve the crystal structures, 1H NMR has been used to determine API/conformer stoichiometry, and diffractograms have been indexed when possible to confirm the crystal form purity.

3.3. New Solid Forms of Compound 1. During the solubility determination of compound 1 in 36 solvents in a range of 30−90 °C, new solvate forms of compound 1 have been discovered and characterized with formic acid (Form A), DMF (Form B), DMSO (Form C), and acetic acid (Forms D-1 to D-4). Compound 1 is soluble at 25 °C in formic acid, DMF, DMSO, and dimethylamine (40% in water). At 40 °C, it is soluble in acetic acid. It is insoluble in methanol, ethanol, isopropanol, butanol, ethylene glycol, ACN, MEK, acetone, MiBK, water, pentane, heptane, cyclohexane, toluene, xylene, AcOEt, diethyl ether, THF, dimethyl ethylene glycol, diisopropyl ether, dioxane, 1,2-dichlorothane, chloroform, benzylalcohol, diethylamine, triethylamine, NH3 (2 M in MeOH), dimethylamine (2 M in MeOH), mixture of MeOH/ DCM (10:90) and trifluoroethanol. The solutions obtained °C until crystallization of a solid. The new forms have been isolated and characterized by means of DSC, 1H NMR, PXRD, and TGA in some cases. All of them show a 1:1 stoichiometry except the system formed by compound 1 and acetic acid, which is a multicomponent solid forms set composed of four different modifications showing polymorphism and different stoichiometries (1:1, 1:2, and 1:4). A complete characterization of each new form is included in the Supporting Information.

All new solvate forms were heated up to a temperature in which the desolvation was ensured under nitrogen atmosphere, then cooled down to room temperature and measured by PXRD, and in all cases the same anhydrous crystal form of compound 1 was obtained. These results together with the fact that no new anhydrous forms of compound 1 were discovered during the solid forms screening suggested initially that compound 1 does not present polymorphism. However, one of the acetic acid solvates (Form D-1) shows a DSC thermogram with a melting point, once the acetic acid is removed on heating, 20 °C lower than the previously observed for compound 1 (Figure 5), which suggests that another

metastable polymorph of compound 1 can exist although with a rapid conversion to the stable one since it has not been isolated so far.

3.4. New Salts/Cocrystals of Compound 1. New multicomponent forms of compound 1 have been identified after the cocrystal screening with 8 out of the 20 coformers tested: 1,4,8,11-tetrazacyclotetradecane, 3,5-dinitrobenzoic acid, gallic acid, orotic acid, 5-nitroisophthalic acid, 3,5-dihydroxybenzoic acid, 1-methyl-2-pyrrolidone, and 4-nitrobenzenesulfonic acid. Some of these new phases were isolated as different polymorphs and solvates. In those cases where crystal structure has not been solved, the definition of the form as a salt or a cocrystal has been done based on the probability of proton transfer determined with eq 1.

- 1:1,4,8,11-Tetrazacyclotetradecane salt (Form I). It has been obtained by reaction crystallization. A 2:1 stoichiometry has been deduced according to 1H NMR and single X-ray diffraction.
- 1:3,5-Dinitrobenzoic acid salt isopropanol solvate (Form II-A): it has been obtained by reaction crystallization in IPA. A 1:1:2 stoichiometry has been deduced according to single X-ray diffraction.
- 1:3,5-Dinitrobenzoic acid salt (Form II-B): it has been obtained by reaction crystallization in acetone. A 1:1 stoichiometry has been deduced according to 1H NMR.
- 1:3,5-Dinitrobenzoic acid salt (Form II-C): it has been obtained by reaction crystallization in THF. A 1:1 or 1:1.5 stoichiometry can be deduced according to 1H NMR.
- 1:3,5-Dinitrobenzoic acid salt dioxane solvate (Form IID): it has been obtained by reaction crystallization in dioxane. A 1:1:1 stoichiometry has been deduced according to 1H NMR.
- 1:3,5-Dinitrobenzoic acid salt (Form II-E): it has been obtained by slurry in water. A 1:1 stoichiometry has been deduced according to 1H NMR.
- 1:Gallic acid salt THF solvate (Form III): It has been obtained by reaction crystallization in THF. A 1:1:1 stoichiometry has been deduced according to 1H NMR. The XRD pattern shows broad diffraction peaks (Figure 6). Further attempts to obtain higher crystallinity solids were unsuccessful.
- 1:Orotic acid salt (Form IV-A): it has been obtained by slurry in IPA (4 days), acetone (4 days), THF (4 days) or dioxane (7 days). A 1:1 stoichiometry has been deduced according to 1H NMR.
- 1:Orotic acid salt (Form IV-B): it has been obtained not pure, as a mixture with Form IV-A, by slurry in dioxane (4 days).

- 1:Orotic acid salt (Form IV-C): it has been obtained not pure, as a mixture with Form IV-A, by slurry in water (4 days).

- 1:5-Nitroisophthalic acid salt (Form V-A): it has been obtained by reaction crystallization in IPA (4 days). A 1:1 stoichiometry has been deduced according to 1HRMN.

- 1:5-Nitroisophthalic acid salt (Form V-B): it has been obtained by reaction crystallization in acetone (4 days). A 1:1 stoichiometry has been deduced according to 1HRMN.

- 1:5-Nitroisophthalic acid salt (Form V-C): it has been obtained by heating up to 215 °C form V−B in a TGA crucible. A 1:1 stoichiometry has been deduced according to 1H-RMN.

- 1:5-Nitroisophthalic acid salt dioxane solvate (Form VD): it has been obtained by reaction crystallization in dioxane (4 days).

- 1:5-Nitroisophthalic acid salt (Form V-E): it has been obtained by heating up to 230 °C form V-D in a TGA instrument. A 1:1 stoichiometry has been deduced according to 1H-RMN.

- 1:3,5-Dihydroxybenzoic acid salt (Form VI): It has been obtained by reaction crystallization in water. A 1:1 stoichiometry has been deduced according to 1H NMR.

- 1:1-Methyl-2-pyrrolidone cocrystal (Form VII): It has been obtained by slurry in THF or heptane. A 1:1 stoichiometry has been deduced according to 1H NMR.

- 1:4-Nitrobenzenesulfonic acid salt (Form VIII): It has been obtained by reaction crystallization in ipOH, acetone, THF, dioxane, or water. A 1:1 stoichiometry has been deduced according to 1H NMR

A comparison of the PXRD of the new multicomponent forms of compound 1 obtained as a single form is shown in Figure 6.

A comparison of the PXRD of the different forms abovementioned for 1:3,5-dinitrobenzoic acid is shown in Figure 7.

A comparison of the PXRD of the different forms abovementioned for 1:orotic acid is shown in Figure 8.

A comparison of the PXRD of the different forms abovementioned for 1:5-nitroisophthalic acid is shown in Figure 9.

When possible, the PXRD diagrams of the new forms were indexed, and the results are shown in Table 3. The rest of the forms could not be obtained in pure form, which hindered the indexing process.

3.5. Single Crystal Structures. Crystals of forms I, II-A, DMF solvate, and acetic acid hybrid salt-cocrystal suitable for SCXRD analysis have been obtained, and their crystallographic data are summarized in Table 4.

3.5.1. Form I. 1:1,4,8,11-Tetrazacyclotetradecane (cyclam) salt crystallizes with one molecule of 1 and half molecule of 1,4,8,11-tetrazacyclotetradecane in the asymmetric unit. The ΔpKa value is 2.0 (pKa of the coformer is 10.9) with a probability of salt formation of P = 62%, and the SCXRD data confirm (from a difference synthesis and refined with an isotropic temperature factor) the location of two hydrogens bonded to the coformer's nitrogen. In the structure, every molecule of 1 anion interacts with a molecule of tetrazacyclotetradecane bis cation and another molecule of 1 via the oxazolidinone ring through charged assisted hydrogen bonds and electrostatic interactions. Moreover, tetrazacyclotetradecane molecules are sandwiched between molecules of 1 using two out of the four amine nitrogens to interact with the 1 oxazolidinone nitrogens.

3.5.2. Acetic Acid Hybrid Salt-Cocrystal. This multicomponent solid form crystallizes with one molecule of 1 and four molecules of acetic acid in the asymmetric unit. The solid form is a hybrid salt-cocrystal37,38 since one molecule of acetic acid has transferred the acidic proton to the pyrimidine nitrogen establishing a charge assisted hydrogen bond and at the same time neutral acetic acid molecules are also present in the crystal structure. Since the ΔpKa value is 1.1 (pKa of the acetic acid is 4.8), the probability of salt formation is P = 47%, and thus this structure could be considered as an example of the "salt-cocrystal continuum". Cocrystals and salts formed between carboxylic acids and N-heterocycles have been analyzed in the literature, and it has been suggested that the formation of unexpected hybrid salt-cocrystals can be produced because carboxylate moieties are not totally satisfied by a single hydrogen-bond donor, which makes necessary the presence of neutral carboxylic acids in the crystal structure.39 In the crystal structure, both C−O distances in the acetate molecule are practically the same (1.263(3) Å and 1.263(2) Å), and the transferred proton well located (and refined with an isotropic temperature factor) on the pyrimidine nitrogen, discarding a potential disorder. Three other acetic acid molecules satisfy the two amide hydrogen bond donors and the CO acceptor groups of 1, which could be anticipated by the position and magnitude of the SSIPs of the isolated compound 1 molecule (Figure 11).

3.5.3. DMF Solvate. The DMF solvate crystallizes with one molecule of 1 and one of DMF in the asymmetric unit. In the structure, molecules of 1 interact in a zigzag arrangement with intermolecular contacts between the oxazolidinone amide and the aminopyrimidine groups. In principle, two configurations are possible: amide/amide plus aminopyrimidine/aminopyrimidine or mixed amide/aminopyrimidine interactions. Interestingly, the interaction energy of both configurations are

very similar when estimated both by pairing H-bond parameters calculated from MMFF94 atomic partial charges ($E = \Sigma ij\ \varepsilon i\varepsilon j$ = 36.7 and 37.2 kJ/mol respectively) and from DFT MEPs ($E = \Sigma ij\ \varepsilon i\varepsilon j$ = 40.5 and 42.7 kJ/mol respectively), the observed configuration being the one with the predicted highest interaction energy. DMF molecules complete the sphere of coordination of 1 by establishing H-bond interactions with the second best donor of 1, Figure 12.

3.5.4. Form II-A. Form II-A crystallizes with one molecule of 1, one of 3,5-dinitrobenzoic acid, and two of isopropanol in the asymmetric unit. Again the crystal form corresponds to a salt in which the pyrimidine ring is protonated and interacts strongly with the carboxylate moiety of the coformer. In the structure only one of the strong SSIPs of 1 (the oxazolidinone NH) is not involved in any relevant intermolecular interaction.

3.6. Polymorphism in the Multicomponent Crystals of 1. Although it has been traditionally suggested that polymorphism in multicomponent crystals is a phenomenon observed with less frequency that in single component crystals,40 it has been put in doubt,41 and recently some of us discovered new cocrystals of agomelatine with polymorphism increasing the list of compounds showing cocrystal polymorphism.42 The present case study shows polymorphism in at least two of the new salts of 1 with 3,5-dinitrobenzoic acid and 5-nitroisophthalic acid, which we believe can contribute to new data to enrich the debate about whether multicomponent crystals are less prone to exhibit polymorphism than single component crystals. In particular, solvates of the 1:3,5- dinitrobenzoic salt II-A and II-D show a DSC thermogram with recrystallization after desolvation of an anhydrous form with a different melting point that anhydrous forms II-B, II-C, and II-E, demonstrating that this salt exists in at least four different polymorphs and two solvates (Figure 14). A similar behavior is observed in solvated salts with 5- nitroisophthalic acid in which forms V-B and V-D are desolvated upon heating in a DSC experiment exhibiting a recrystallization exothermic process which produced two different solid forms according to the melting points.

4. CONCLUSIONS

By using a holistic cocrystallization screen approach, we have explored the formulation landscape of the first inhaled JAKSTAT inhibitor 1 and have generated multiple solid forms covering a broad physicochemical space and therefore decreased the risk of future potential development failures due to a nonoptimal pharmacokinetic lung profile or undesired lung effects in humans. This comprehensive cocrystal/salts screening was conducted using different combinations of solvents at several concentrations and temperatures, with variable cooling rates, in both thermodynamic and kinetic conditions. Solubility of 1 was initially determined in 30 solvents, and accordingly drop grinding, reaction crystallization, and slurry techniques were applied to each 1/conformer combination. Despite 1 not showing polymorphism, eight new forms of 1 (and multiple solvates) were identified: 1,4,8,11-tetrazacyclotetradecane, 3,5-dinitrobenzoic acid, gallic acid, orotic acid, 5-nitroisophthalic acid, 3,5-dihydroxybenzoic acid, 1-methyl-2-pyrrolidone, and 4-nitrobenzenesulfonic acid. Many of these new phases were isolated as different polymorphs and solvates. All solids were analyzed by PXRD to assess the formation of a new solid form. After a careful comparison and risk assessment of the in vivo pharmacokinetics, lung deposition, clearance, pulmonary response, effect and safety profile, “the best” one will be progressed as the candidate drug into human trials. We are now assessing their in vivo potential where the most promising ones will be scaled up and brought forward to the next phase, and this will be the subject of a future publication.

References

Leonard, W. J.; Lin, J.-X. Cytokine receptor signaling pathways. J. Allergy Clin. Immunol. 2000, 105, 877−888.

Rawlings, J. S.; Rosler, K. M.; Harrison, D. A. The JAK/STAT signaling pathway. J. Cell Sci. 2004, 117, 1281−1283.

Kudlacz, E.; Perry, B.; Sawyer, P.; Conklyn, M.; McCurdy, S.; Brissette, W.; Flanagan, M.; Changelian, P. The novel JAK-3 inhibitor CP-690550 is a potent immunosuppressive agent in various murine models. Am. J. Transplant. 2004, 4, 51−57.

Changelian, P. S.; Flanagan, M. E.; Ball, D. J.; Kent, C. R.; Magnuson, K. S.; Martin, W. H.; Rizzuti, B. J.; Sawyer, P. S.; Perry, B. D.; Brissette, W. H.; McCurdy, S. P.; Kudlacz, E. M.; Conklyn, M. J.; Elliott, E. A.; Koslov, E. R.; Fisher, M. B.; Strelevitz, T. J.; Yoon, K.; Whipple, D. A.; Sun, J.; Munchhof, M. J.; Doty, J. L.; Casavant, J. M.; Blumenkopf, T. A.; Hines, M.; Brown, M. F.; Lillie, B. M.; Subramanyam, C.; Chang, S.-P.; Milici, A. J.; Beckius, G. E.; Moyer, J. D.; Su, C.; Woodworth, T. G.; Gaweco, A. S.; Beals, C. R.; Littman, B. H.; Fisher, D. A.; Smith, J. F.; Zagouras, P.; Magna, H. A.; Saltarelli, M. J.; Johnson, K. S.; Nelms, L. F.; Des Etages, S. G.; Hayes, L. S.; Kawabata, T. T.; Finco-Kent, D.; Baker, D. L.; Larson, M.; Si, M.-S.; Paniagua, R.; Higgins, J.; Holm, B.; Reitz, B.; Zhou, Y.-J.; Morris, R. E.; O'Shea, J. J.; Borie, D. C. Prevention of Organ Allograft Rejection by a Specific Janus Kinase 3 Inhibitor. Science (Washington, DC, U. S.) 2003, 302, 875−878.

Harrison, D. A. The JAK/STAT pathway. Cold Spring Harbor Perspect. Biol. 2012, 4 (3), a011205.

Frank, D. A. STAT signaling in the pathogenesis and treatment of cancer. Mol. Med. (N. Y.) 1999, 5, 432−456.

Seidel, H. M.; Lamb, P.; Rosen, J. Pharmaceutical intervention in the JAK/STAT signaling pathway. Oncogene 2000, 19, 2645−2656.

Clark, J. D.; Flanagan, M. E.; Telliez, J.-B. Discovery and Development of Janus Kinase (JAK) Inhibitors for Inflammatory Diseases. J. Med. Chem. 2014, 57, 5023−5038.

Vijayakrishnan, L.; Venkataramanan, R.; Gulati, P. Treating inflammation with the Janus Kinase inhibitor CP-690,550. Trends Pharmacol. Sci. 2011, 32, 25−34.

Baeckman, P.; Tehler, U.; Olsson, B. Predicting Exposure After Oral Inhalation of the Selective Glucocorticoid Receptor Modulator, AZD5423, Based on Dose, Deposition Pattern, and

371 Mechanistic Modeling of Pulmonary Disposition. J. Aerosol Med. Pulm. Drug Delivery 2017, 30,
372 108−117.

373 Forbes, B.; Backman, P.; Christopher, D.; Dolovich, M.; Li, B. V.; Morgan, B. In Vitro Testing for
374 Orally Inhaled Products: Developments in Science-Based Regulatory Approaches. AAPS J. 2015,
375 17, 837−52.

376 Jones, R. M.; Neef, N. Interpretation and prediction of inhaled drug particle accumulation in the lung
377 and its associated toxicity. Xenobiotica 2012, 42, 86−93.

378 Hunter, C. A.; Prohens, R. Solid form and solubility. CrystEngComm 2017, 19, 23−26.

379 Good, D. J.; Rodriguez-Hornedo, N. Solubility Advantage of Pharmaceutical Cocrystals. Cryst. Growth
380 Des. 2009, 9, 2252−2264.

381 Cresset torchV10lite, http://www.cresset-group.com/products/ torch/torchlite/.

382 Frisch, M. J.; Trucks, G. W.; Schlegel, H. B.; Scuseria, G. E.; Robb, M. A.; Cheeseman, J. R.; Scalmani,
383 G.; Barone, V.; Mennucci, B.; Petersson, G. A.; Nakatsuji, H.; Caricato, M.; Li, X.; Hratchian, H.
384 P.; Izmaylov, A. F.; Bloino, J.; Zheng, G.; Sonnenberg, J. L.; Hada, M.; Ehara, M.; Toyota, K.;
385 Fukuda, R.; Hasegawa, J.; Ishida, M.; Nakajima, T.; Honda, Y.; Kitao, O.; Nakai, H.; Vreven, T.;
386 Montgomery, J. A., Jr.; Peralta, J. E.; Ogliaro, F.; Bearpark, M.; Heyd, J. J.; Brothers, E.; Kudin,
387 K. N.; Staroverov, V. N.; Kobayashi, R.; Normand, J.; Raghavachari, K.; Rendell, A.; Burant, J.
388 C.; Iyengar, S. S.; Tomasi, J.; Cossi, M.; Rega, N.; Millam, J. M.; Klene, M.; Knox, J. E.; Cross,
389 J. B.; Bakken, V.; Adamo, C.; Jaramillo, J.; Gomperts, R.; Stratmann, R. E.; Yazyev, O.; Austin,
390 A. J.; Cammi, R.; Pomelli, C.; Ochterski, J. W.; Martin, R. L.; Morokuma, K.; Zakrzewski, V. G.;
391 Voth, G. A.; Salvador, P.; Dannenberg, J. J.; Dapprich, S.; Daniels, A. D.; Farkas, O.; Foresman,
392 J. B.; Ortiz, J. V.; Cioslowski, J.; Fox, D. J. Gaussian 09; Gaussian, Inc.: Wallingford, CT, 2009.

393 Calero, C. S.; Farwer, J.; Gardiner, E. J.; Hunter, C. A.; Mackey, M.; Scuderi, S.; Thompson, S.; Vinter,
394 J. G. Footprinting molecular electrostatic potential surfaces for calculation of solvation energies.
395 Phys. Chem. Chem. Phys. 2013, 15, 18262−18273.

396 Boultif, A.; Louer, D. Powder pattern indexing with the dichotomy method. J. Appl. Crystallogr. 2004,
397 37, 724−731.

398 Le Bail, A.; Duroy, H.; Fourquet, J. L. The ab-initio structure determination of lithium antimony
399 tungstate (LiSbWO6) by x-ray powder diffraction. Mater. Res. Bull. 1988, 23, 447−52.
400 Rodriguez-Carvajal, J. Recent advances in magnetic structure determination by neutron powder
401 diffraction. Phys. B (Amsterdam, Neth.) 1993, 192, 55−69.

SADABS; Bruker AXS: Madison, Wisconsin, USA, 2004; SAINT, Software Users Guide, Version 6.0; Bruker Analytical X−ray Systems: Madison, WI, 1999. Sheldrick, G. M. SADABS v2.03: Area-Detector Absorption Correction: University of Göttingen: Göttingen, Germany, 1999; Saint Version 7.60A (Bruker AXS 2008); SADABS V. 2008-1, 2008.

Sheldrick, G. M. A short history of SHELX. Acta Crystallogr., Sect. A: Found. Crystallogr. 2008, 64, 112−122.

Musumeci, D.; Hunter, C. A.; Prohens, R.; Scuderi, S.; McCabe, J. F. Virtual cocrystal screening. Chem. Sci. 2011, 2, 883−890.

Grecu, T.; Hunter, C. A.; Gardiner, E. J.; McCabe, J. F. Validation of a Computational Cocrystal Prediction Tool: Comparison of Virtual and Experimental Cocrystal Screening Results. Cryst. Growth Des. 2014, 14, 165−171.

Grecu, T.; Adams, H.; Hunter, C. A.; McCabe, J. F.; Portell, A.; Prohens, R. Virtual Screening Identifies New Cocrystals of Nalidixic Acid. Cryst. Growth Des. 2014, 14, 1749−1755.

Grecu, T.; Prohens, R.; McCabe, J. F.; Carrington, E. J.; Wright, J. S.; Brammer, L.; Hunter, C. A. CrystEngComm 2017, 19, 3592−3599.

Llinas, A.; Barbas, R.; Font-Bardia, M.; Quayle, M. J.; Velaga, S.; Prohens, R. Two New Polymorphic Cocrystals of Zafirlukast: Preparation, Crystal Structure, and Stability Relations. Cryst. Growth Des. 2015, 15, 4162−4169.

Corner, P.; Berry, D. J.; McCabe, J. F.; Barbas, R.; Prohens, R.; Du, H.; Zhou, H.; Llinas, A. Property Prediction and Pharmacokinetic Evaluation of Mixed Stoichiometry Cocrystals of Zafirlukast, a Drug Delivery Case Study. CrystEngComm 2018, 20, 1346−1351.

Calero, C. S.; Farwer, J.; Gardiner, E. J.; Hunter, C. A.; Mackey, M.; Scuderi, S.; Thompson, S.; Vinter, J. G. Footprinting molecular electrostatic potential surfaces for calculation of solvation energies. Phys. Chem. Chem. Phys. 2013, 15, 18262−18273.

Oliver, A.; Hunter, C. A.; Prohens, R.; Rossello, J. L. A surface site interaction point methodology for macromolecules and huge molecular databases. J. Comput. Chem. 2017, 38, 419−426.0

Oliver, A.; Hunter, C. A.; Prohens, R.; Rossello, J. L. An improved methodology to compute Surface Site Interaction Points using high density Molecular Electrostatic Potential Surfaces. J. Comput. Chem. 2018, 39, 2371−2377.

Childs, S. L.; Stahly, G. P.; Park, A. The salt-cocrystal continuum: the influence of crystal structure on ionization state. Mol. Pharmaceutics 2007, 4, 323−338.

Lemmerer, A.; Govindraju, S.; Johnston, M.; Motloung, X.; Savig, K. L. Co-crystals and molecular salts of carboxylic acid/pyridine complexes: can calculated pKa's predict proton transfer? A case study of nine complexes. CrystEngComm 2015, 17, 3591−3595.

Cruz-Cabeza, A. J. Acid-base crystalline complexes and the pKa rule. CrystEngComm 2012, 14, 6362−6365.

Apparent pKa's calculated using ACD Labs software, release 2015 Pack2, 09 Jun 2015.

Methanol, ethanol, IPA, butanol, ethylene glycol, 2,2,2- trifluoroethanol, benzyl alcohol, ACN, MEK, acetone, MiBK, water, DMF, DMSO, pentane, heptane, cyclohexane, toluene, xylene, AcOEt, diethylether, THF, dimethyl ethylene glycol, diisopropyl ether, dioxane, dichloromethane, chloroform, formic acid, acetic acid, NH3 (32%) in water, NH3 (2.0 M) in methanol, dimethylamine (2.0 M) in methanol, diethylamine, diethylamine (32%) in water, trimethylamine. and methanol-dichloromethane (10:90).

Jacobs, A.; Amombo Noa, F. M. Hybrid Salt-Cocrystal Solvate: p-Coumaric Acid and Quinine System. J. Chem Crystallogr. 2014, 44, 57−62.

Mahieux, J.; Gonella, S.; Sanselme, M.; Coquerel, G. Crystal structure of a hybrid salt−cocrystal and its resolution by preferential crystallization: ((±)-trans-N,N′-dibenzyldiaminocyclohexane)(2,3-dichlorophenylacetic acid)4. CrystEngComm 2012, 14, 103−111.

Aakeröy, C. B.; Fasulo, M. E.; Desper, J. Cocrystal or Salt: Does It Really Matter? Mol. Pharmaceutics 2007, 4 (3), 317−322.

Reddy, L. S.; Babu, N. J.; Nangia, A. Chem. Commun. (Cambridge, U. K.) 2006, 0, 1369−1371.

Lemmerer, A.; Adsmond, D. A.; Esterhuysen, C.; Bernstein, J. Polymorphic Co-crystals from Polymorphic Co-crystal Formers: Competition between Carboxylic Acid···Pyridine and Phenol···Pyridine Hydrogen Bonds. Cryst. Growth Des. 2013, 13, 3935−3952.

Prohens, R.; Barbas, R.; Portell, A.; Font-Bardia, M.; Alcobe, X.; Puigjaner, C. Polymorphism of Cocrystals: The Promiscuous Behavior of Agomelatine. Cryst. Growth Des. 2016, 16, 1063−1070.

Legends to figures

Fig. 1 Molecular structure of compound 1.

Fig. 2 SSIPs calculated for 1. Blue spheres correspond to H-bond donors and red spheres to H-bond acceptors

Fig. 3 Powder X-ray diffractograms of compound 1 solvates (blue: Form A, red: Form B, green: Form C).

Fig. 4 Powder X-ray diffractograms of compound 1 acetic acid solvates (blue: Form D-1, red: Form D-2, green: Form D-3, brown: Form D-4).

Fig. 5 DSC (top) and TGA (bottom) of 1/acetic acid forms.

Fig. 6 Powder X-ray diffractograms of the new multicomponent forms of compound 1 obtained as a single form (blue: Form I, red: Form III, green: Form VI, brown: Form VII, purple: Form VIII).

Fig. 7 Powder X-ray diffractograms of the new forms of 1:3,5-dinitrobenzoic acid (blue: Form II-A, red: Form II−B, green: Form II−C, brown: Form II-D, purple: Form II-E).

Fig. 8 Powder X-ray diffractograms of the new forms of 1:orotic acid (blue: Form IV-A, red: mixture Form IV-A and Form IV−B, green: mixture Form IV-A and Form IV-C).

Fig. 9 Powder X-ray diffractograms of the new forms of 1:5-nitroisophthalic acid (blue: Form V-A, red: Form V−B, green: Form V−C, brown: Form V-D, purple: Form V-E).

Fig. 10 (a) Electrostatic interactions in the sandwiched 1,4,8,11-tetrazacyclotetradecane cation and (b) ribbons of 1 molecules assembled by charge assisted hydrogen bonds.

Fig 11 Contacts observed in the crystal structure of acetic acid hybrid salt-cocrystal.

Fig. 12 (a) 1 H-bond parameters from DFT calculations and (b) contacts observed in the crystal structure of DMF solvate

Fig. 13 Interactions of 1 in the crystal structure of Form II-A.

Fig. 14 DSC (top) and TGA (bottom) of 1:3,5-dinitrobenzoic salts.

Fig. 15 DSC (top) and TGA (bottom) of 1:5-nitroisophthalic acid salts.

FIGURE 1

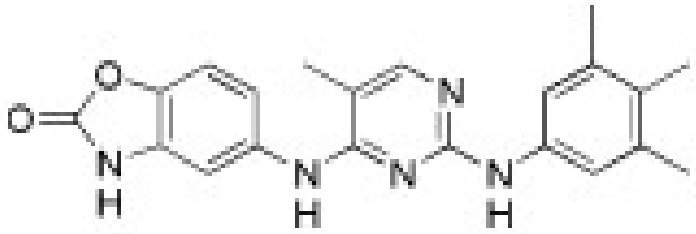

507 **FIGURE** 2

508

509

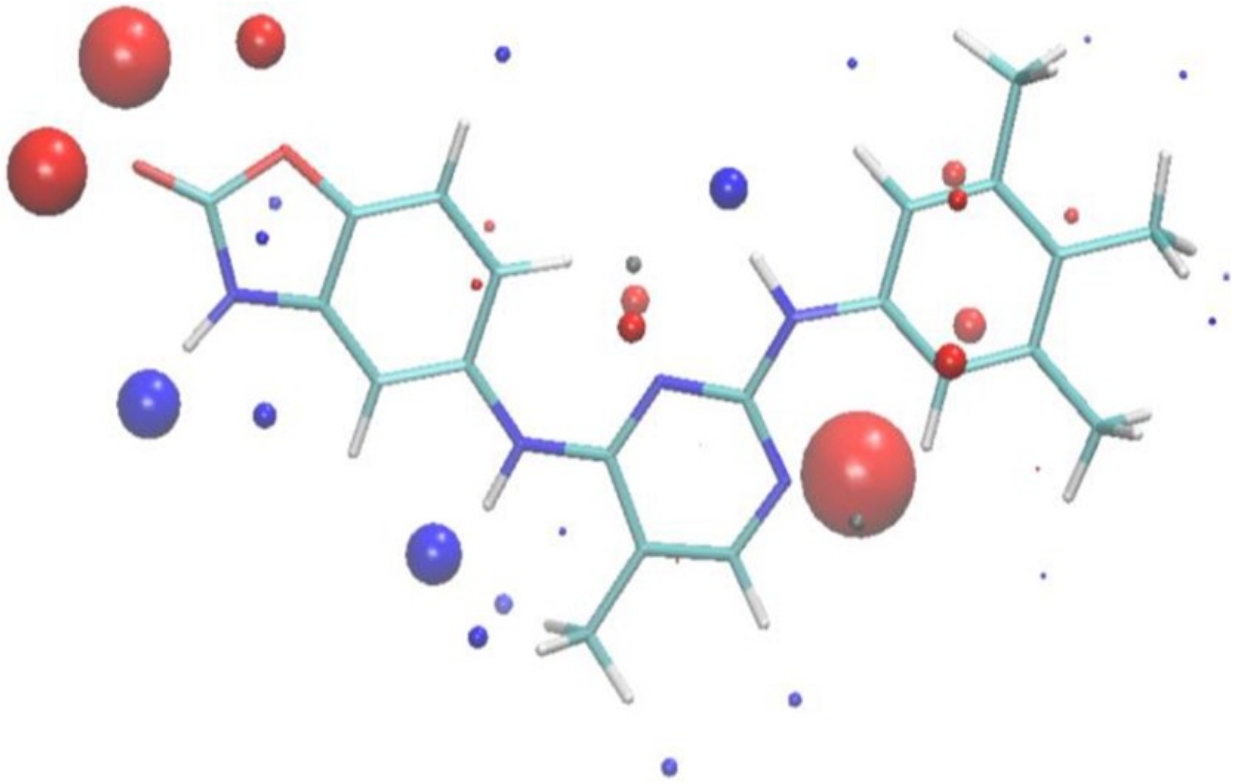

510

511

512 **FIGURE** 3

513

514

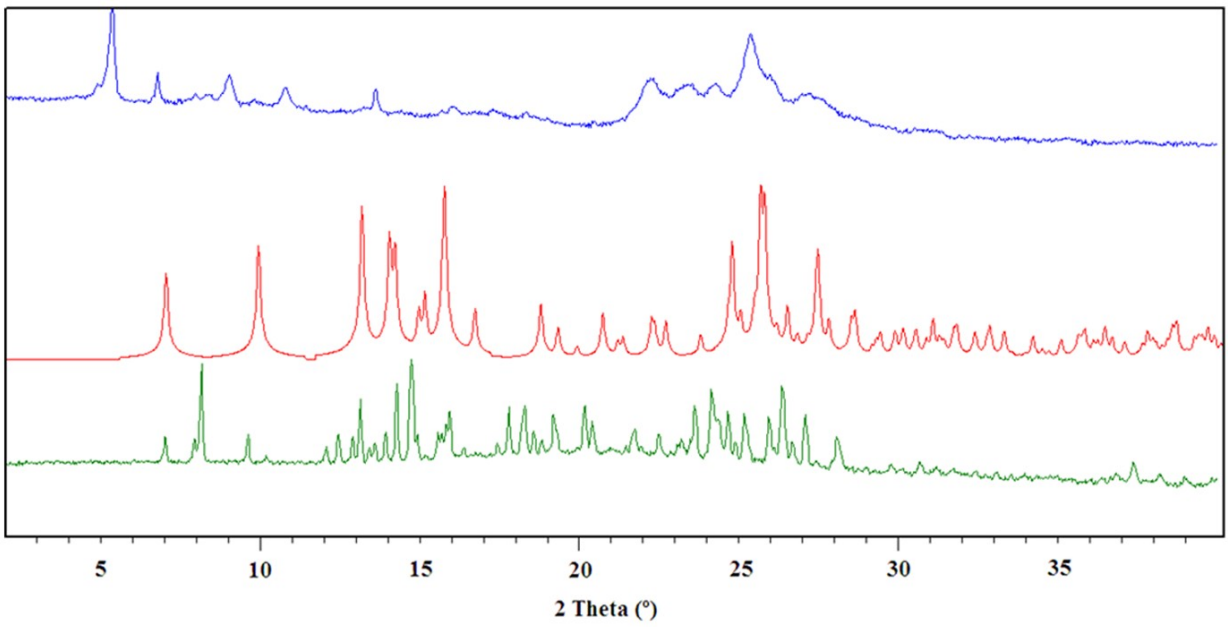

515

516

517 **FIGURE 4**

518

519

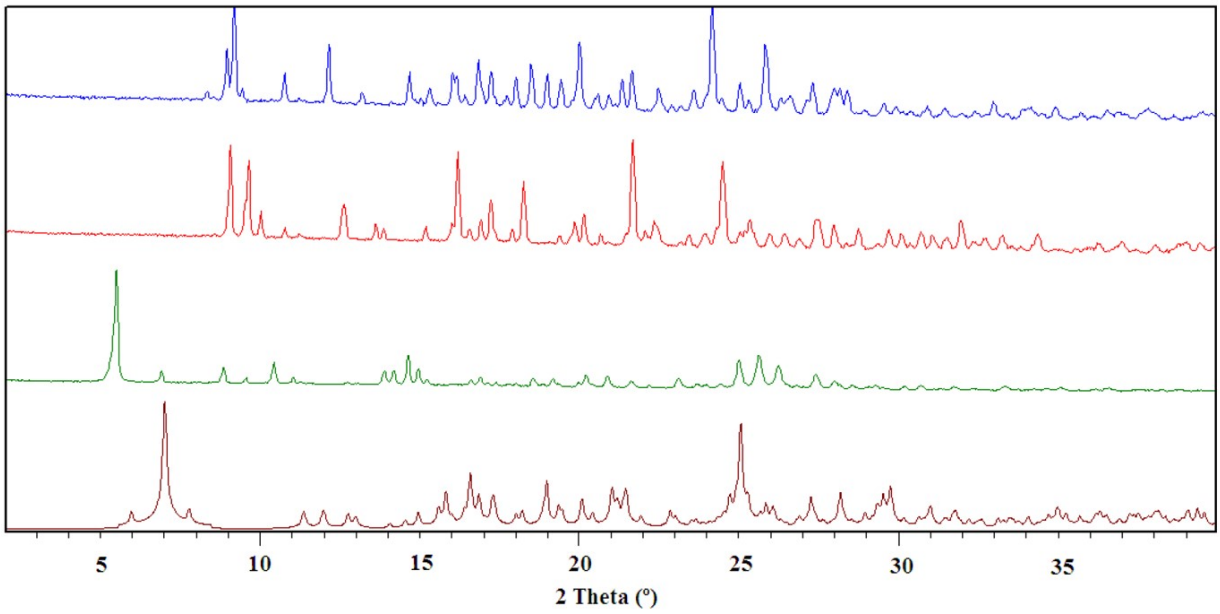

520

521

FIGURE 5

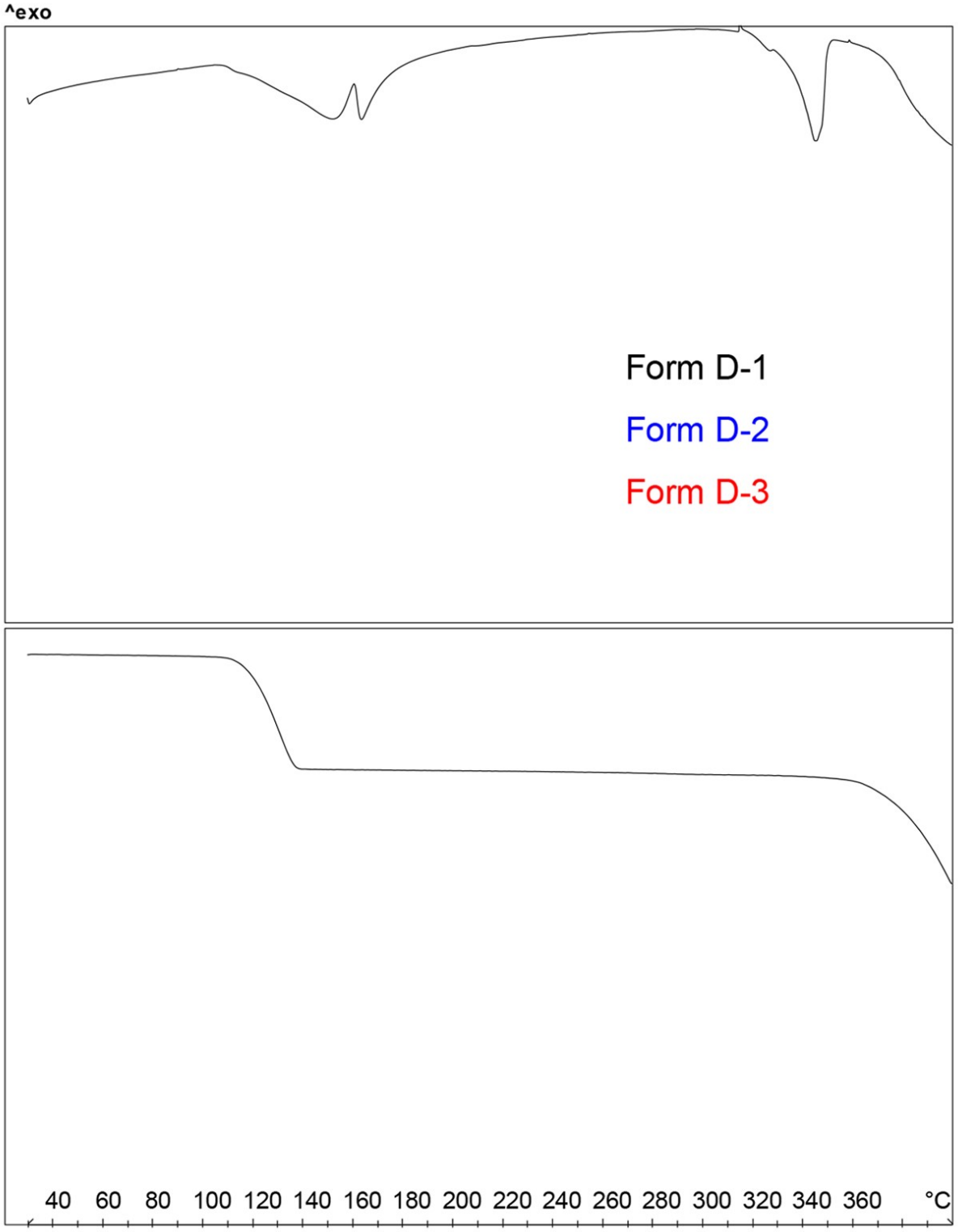
^exo
Form D-1
Form D-2
Form D-3
40 60 80 100 120 140 160 180 200 220 240 260 280 300 320 340 360 °C

528 **FIGURE 6**

529

530

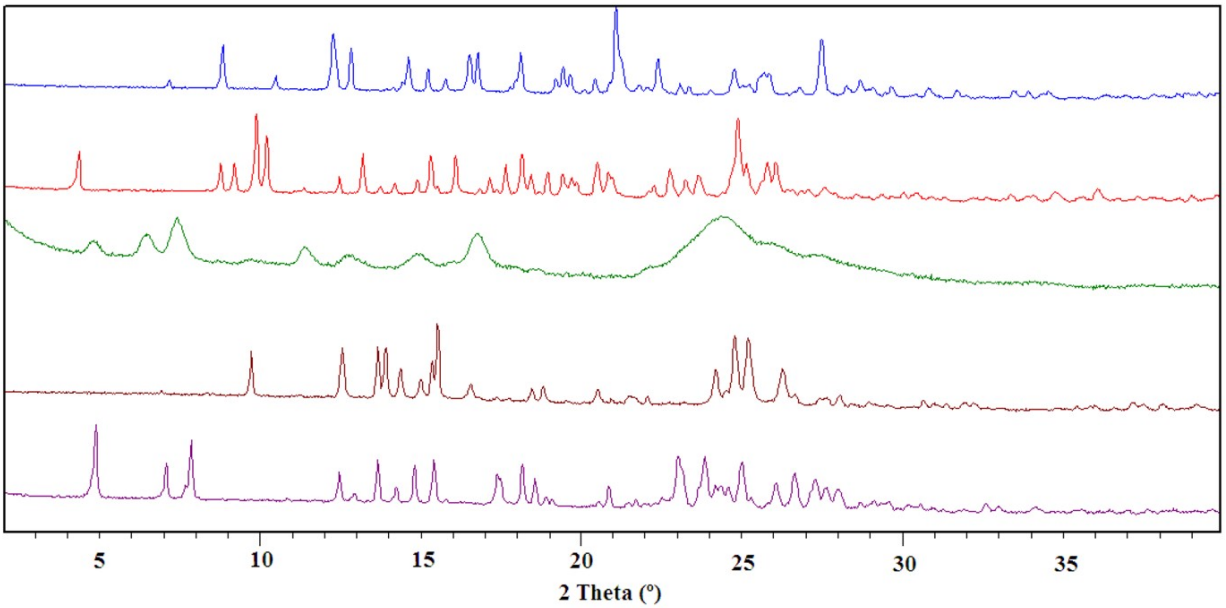

531

532

FIGURE 7

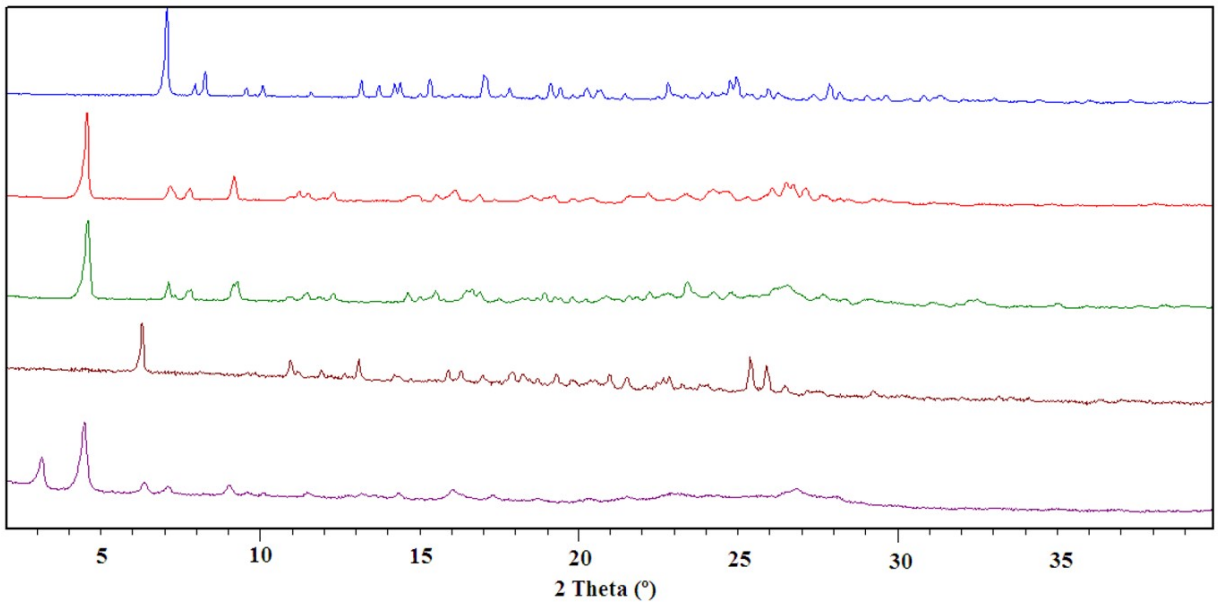

538 **FIGURE 8**

539

540

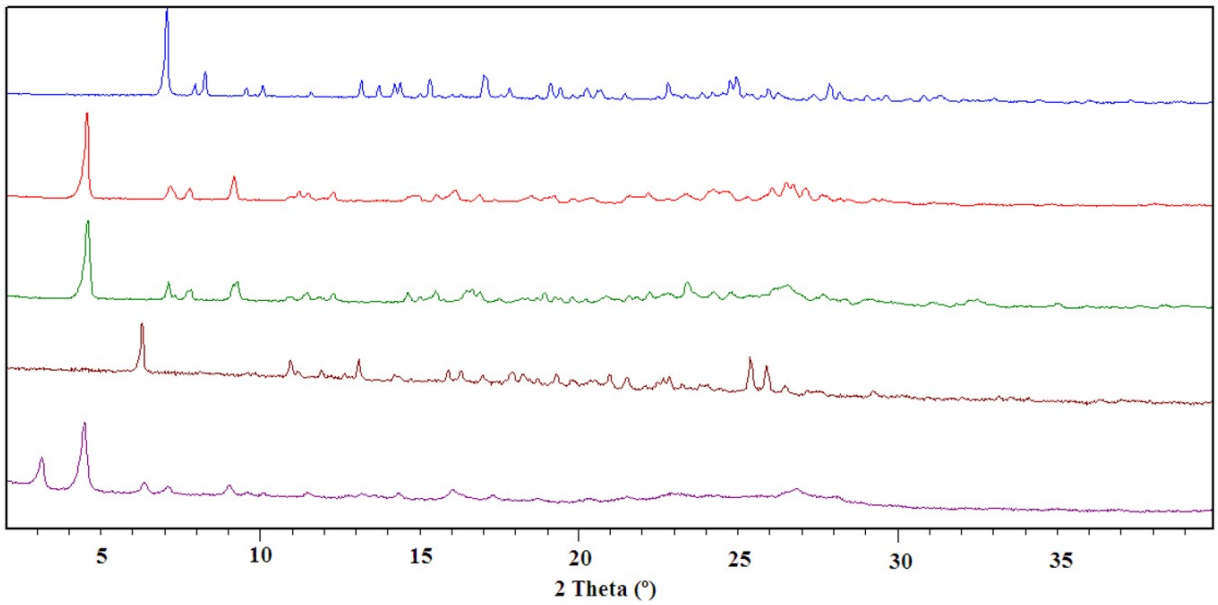

541

542

FIGURE 9

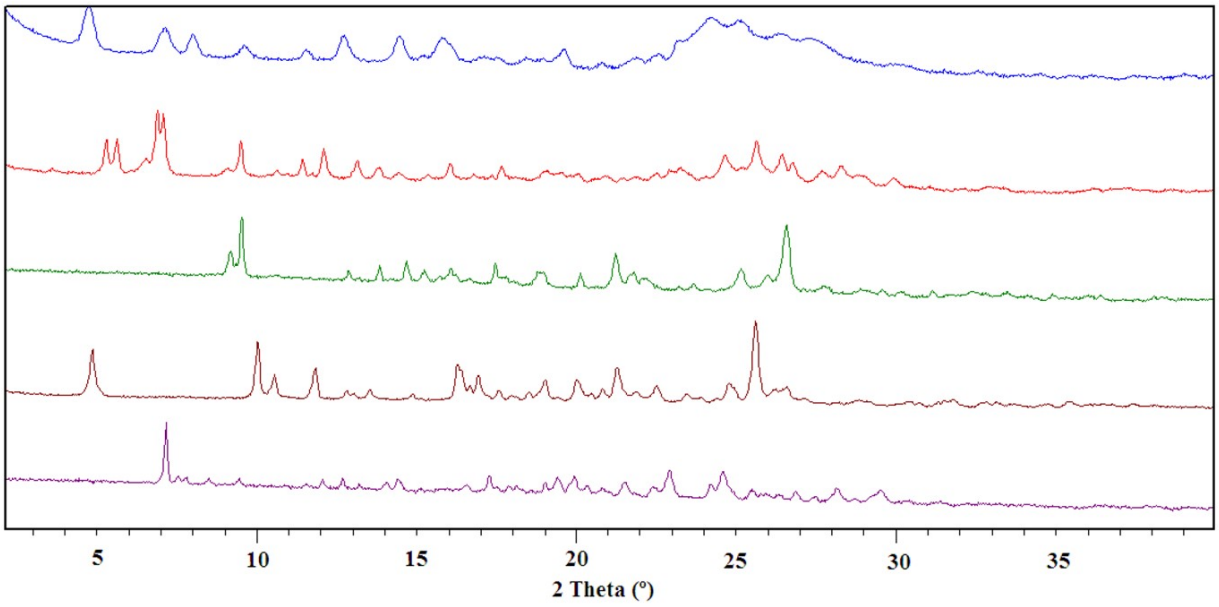

548 **FIGURE 10**

549

550

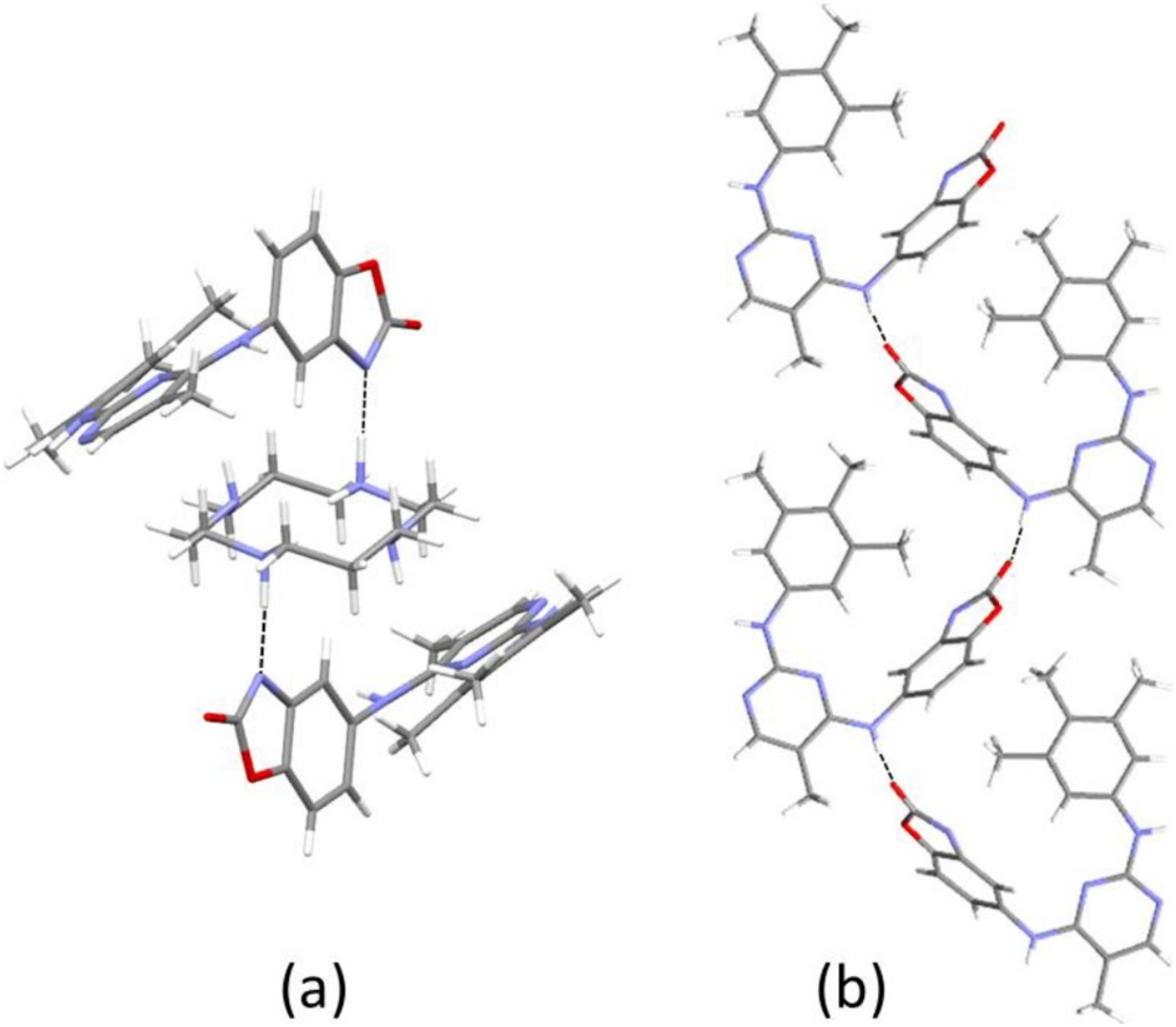

551

552

553

554

555 **FIGURE 11**

556

557

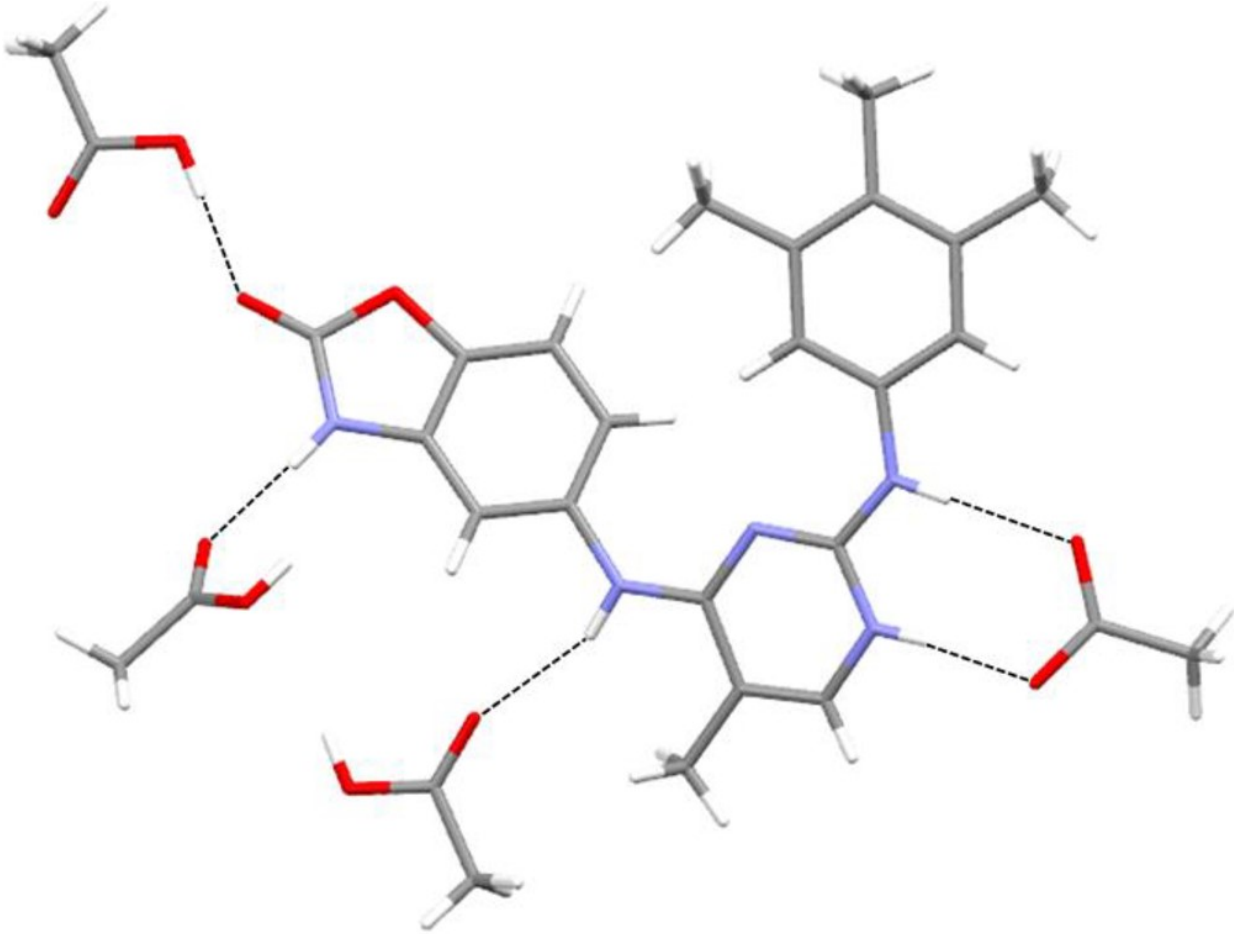

558

559

560

561 **FIGURE 12**

562

563

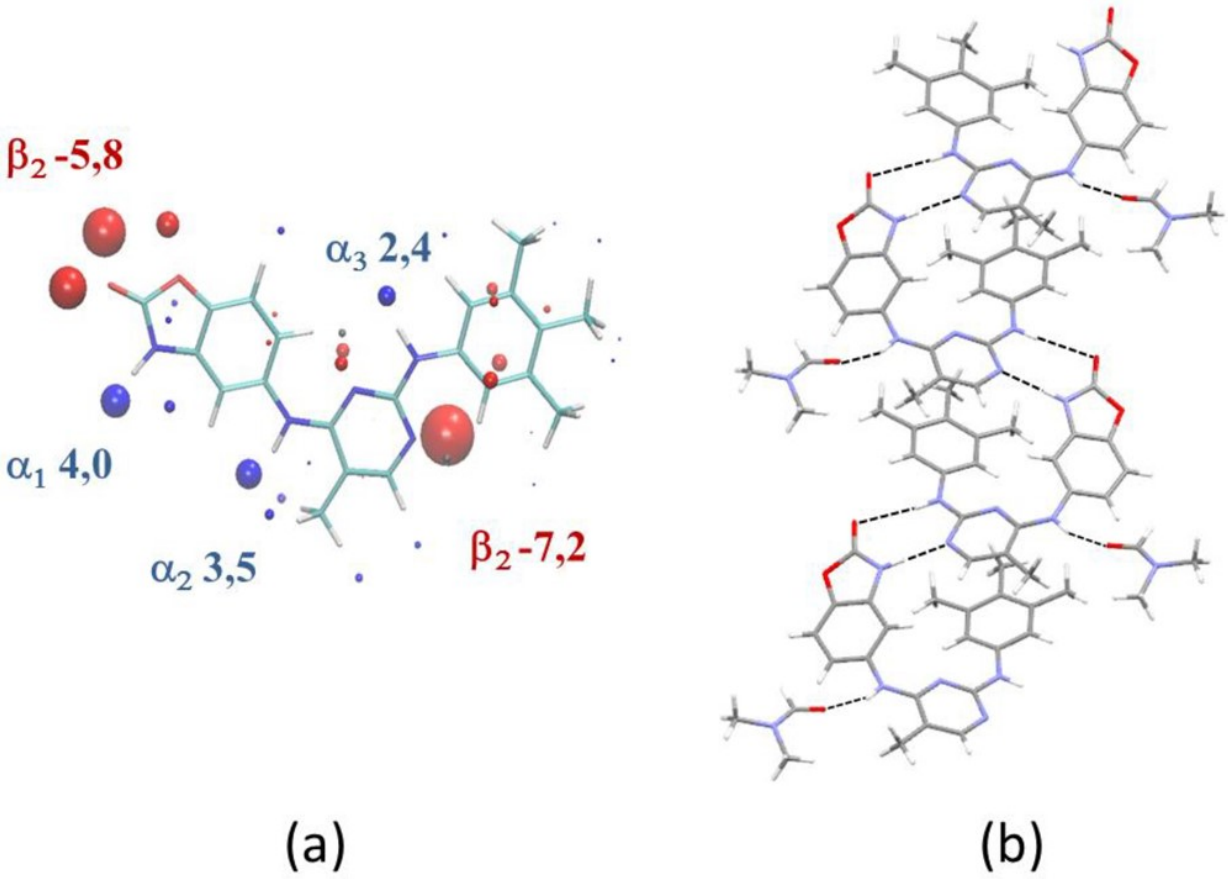

564

565

566

FIGURE 13

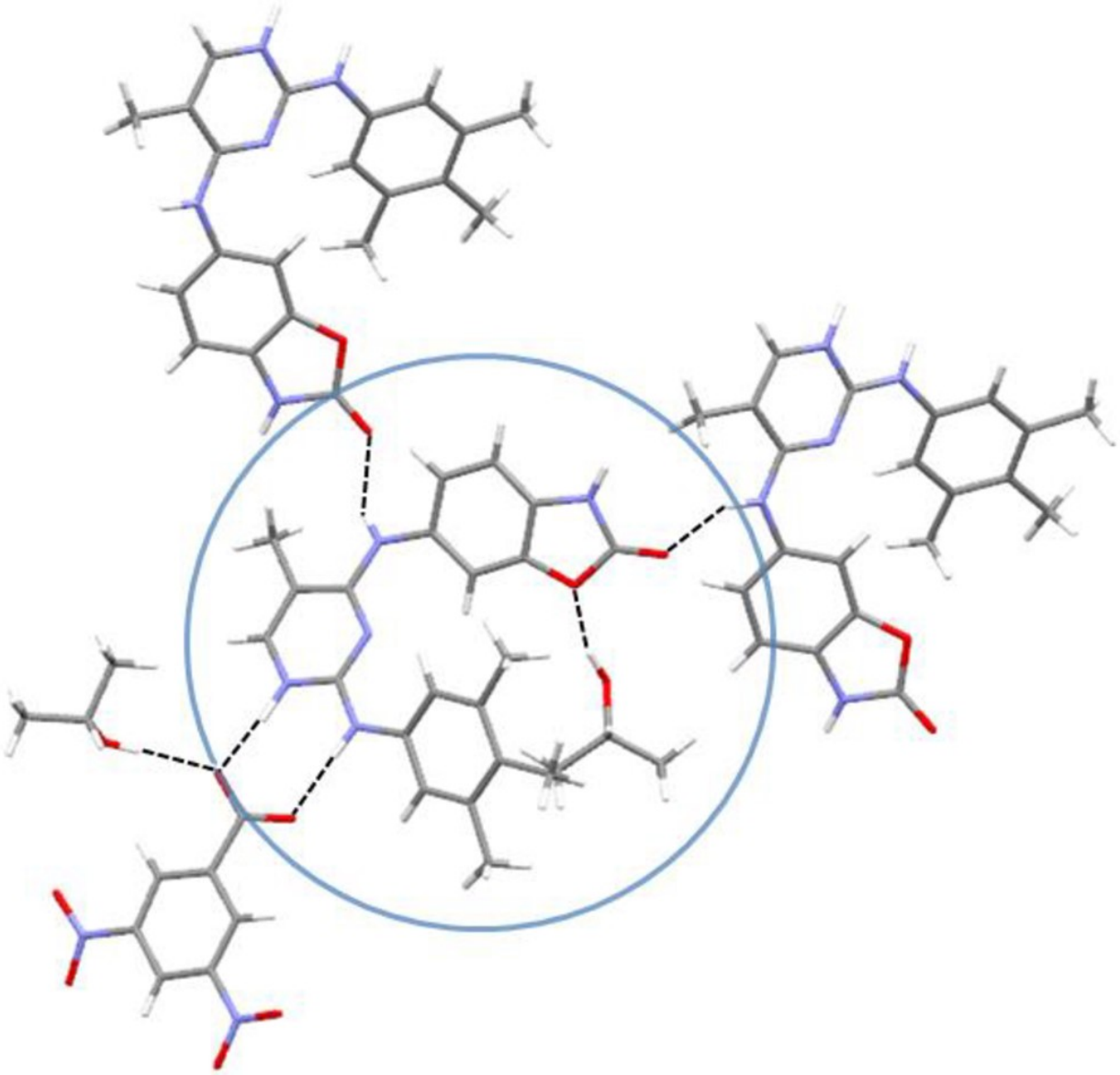

FIGURE 14

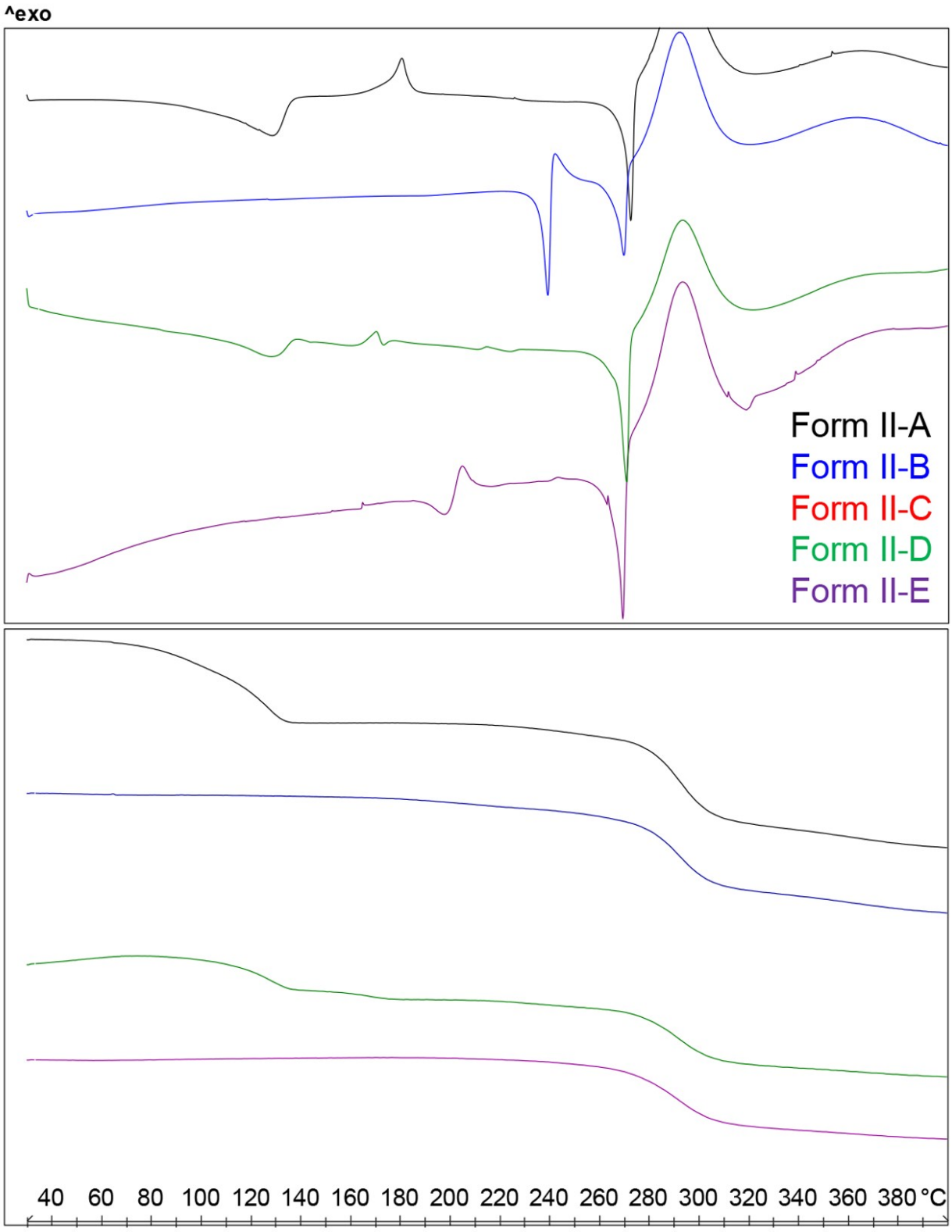
^exo
Form II-A
Form II-B
Form II-C
Form II-D
Form II-E
40 60 80 100 120 140 160 180 200 220 240 260 280 300 320 340 360 380 °C

Table 1 Table 1. Summary of Physicochemical Properties of the Free Base of 1

molecular weight (g/mol)	375.4
LogD	4.2
crystalline solubility (μM)	0.03
experimental pK_{a1}, pK_{a2}	5.9, 8.9
Hu PPB (% free)	0.16
Hu Caco2 pH = 6.5 with inhibitors ($\times$ 1 $\times$ 10^{-6} cm/s)	11.2

Table 2 Cocrystal Screening Coformers Ranked by ΔE, pKa'sa

Coformer	ΔE / kJ mol^{-1}	Calculated coformer pKa[35]	ΔpKa	P (%)
Triphenylphosphine Oxide	28.2	-	-	-
1,10-Phenanthroline	27.6	4.9	-4.0	0
1,4-Diazabicyclo[2.2.2]octane	22.3	8.2	-0.7	16
1,4,8,11-Tetrazacyclotetradecane	18.0	10.9	2.0	62
N,N-Dimethylpiperazine	14.5	8.0	-0.9	13
3,5-Dinitrobenzoic acid	14.4	2.8	3.1	81
(+) – Nootkatone	13.7	-	-	-
1,1-Diethoxyethane	13.3	-	-	-
1-Methyl-2-pyrrolidinone	13.0	-0.4	-9.3	0
1-Methylimidazole	12.9	7.0	-1.9	0
4-Nitrobenzenesulfonic acid	12.0	-1.4	7.3	100
Gallic acid	11.1	4.3	1.6	55
Quercetin	10.7	6.3	-0.4	21
Acetylpyrazine	10.7	0.3	-8.6	0
5-Nitroisophthalic acid	10.6	2.8	3.1	81
Orotic acid	10.4	2.8	3.1	81
Tetracyanoethylene	9.0	-	-	-
Pentaflorophenol	8.8	5.5	0.4	35
Resorcinol	8.0	9.4	-3.5	0
3,5-Dihydroxybenzoic acid	7.2	3.9	2.0	62

[a]Red = acidic group, blue = basic group.

Table 3. Indexed Unit Cell Parameters Data of Compound 1 Multicomponent Forms

form	a (Å)	b (Å)	c (Å)	α (deg)	β (deg)	γ (deg)	V (Å^3)	R_{wp} (%)	space group
D-2	12.123(2)	17.606(3)	11.136(2)	90	105.95(1)	90	2285.3(8)	8.2	$P2_1/n$
III	20.793(4)	10.906(1)	16.091(3)	90	104.80(1)	90	3527(1)	6.8	$P2_1/c$
IV-A	30.07(1)	22.592(9)	4.308(2)	90	116.47(4)	90	2619(2)	8.3	$P2_1/a$
V-D	18.422(8)	10.011(5)	10.972(3)	116.80(2)	87.75(2)	99.29(3)	1781(1)	7.8	$P\bar{1}$
VII	13.201(5)	12.683(4)	7.498(2)	90	101.73(2)	90	1229.2(7)	9.3	$P2/n$

595 **Table 4**. Crystal Data for the Different Crystal Forms of Compound 1

596

structure	Form I	Form II-A	DMF solvate	acetic acid hybrid salt-cocrystal
empirical formula	$C_{26}H_{33}N_7O_2$	$C_{34}H_{41}N_7O_{10}$	$C_{24}H_{28}N_6O_3$	$C_{29}H_{37}N_5O_{10}$
formula weight	475.59	707.74	448.52	615.63
temperature (K)	100(2)	100(2)	100(2)	100(2)
wavelength (Å)	0.71073	0.71073	1.54178	0.71073
crystal system	monoclinic	monoclinic	monoclinic	triclinic
space group	$P2_1/c$	$P2_1/n$	Pn	$P\bar{1}$
a, b, c (Å)	12.4888(17)	11.4419(8)	7.2802(5)	7.8386(12)
	13.8659(18)	15.2684(12)	12.5393(9)	13.257(2)
	14.4933(19)	21.4335(17)	12.7893(10)	15.457(3)
α, β, γ (deg)	90	90	90	72.782(6)
	103.322(5)	103.182(3)	99.226(4)	86.818(6)
	90	90	90	82.655(7)
volume (Å^3)	2442.2(6)	3645.8(5)	1152.41(15)	1521.4(4)
Z, density (calc.) (Mg/m^3)	4, 1.293	4, 1.289	2, 1.293	2, 1.344
crystal size (mm^3)	0.501 × 0.312 × 0.261	0.522 × 0.091 × 0.040	0.862 × 0.488 × 0.305	0.460 × 0.072 × 0.070
reflections collected/unique	77204/9331 [R(int)= 0.0448]	123319/9088 [R(int) = 0.1079]	20741/4169 [R(int) = 0.0681]	53225/7000 [R(int) = 0.1322]
data/parameters	9331/0/335	9088/397/522	4169/3/322	7000/0/409
goodness-of-fit on F^2	1.046	1.036	1.023	1.032
final R indices [$I > 2\sigma(I)$]	R_1 = 0.0479, wR_2 = 0.1409	R_1 = 0.0601, wR_2 = 0.1510	R_1 = 0.0465, wR_2 = 0.1026	R_1 = 0.0571, wR_2 = 0.1067
CCDC	1868808	1868809	1868807	1868806

597